Original Research Paper

The influence of the chemical surface composition on the drying process of milk droplets

Martin Foerster [a], Thomas Gengenbach [b], Meng Wai Woo [a], Cordelia Selomulya [a,*]

[a] Department of Chemical Engineering, Monash University, Clayton, Victoria 3800, Australia
[b] CSIRO Manufacturing, Bayview Avenue, Clayton, Victoria 3168, Australia

ABSTRACT

The functional properties of multi-component particles are strongly affected by their chemical surface composition, for instance in pharmaceutical and food applications. The powders are often produced from emulsions and solutions by convective drying, such as spray drying. A detailed understanding of the drying and shrinkage kinetics of the material is hereby crucial to optimise process design and product characteristics. In this study, a modified analysis technique was implemented into filament single droplet drying to observe the changes in component distribution of two milk model emulsions with drying time as well as the impact thereof on the water evaporation resistance and shrinkage behaviour. The drying droplets were cryogenically flash-frozen at discrete drying times and, subsequent to freeze-drying, investigated in terms of their chemical surface composition and internal fat and protein distribution. The droplets of a high-fat milk model emulsion were covered by a continuous fat film throughout the whole drying process, whereas the droplets of a low-fat model emulsion featured a surface overrepresentation of protein in comparison to the bulk concentration. The protein further enriched near the surface with increasing drying time. In the high-fat system, the lipid surface film reduced the extent of particle shrinkage and impeded the drying process.

Crown Copyright © 2016 The Society of Powder Technology Japan. Published by Elsevier B.V. All rights reserved.

1. Introduction

A high content of fat on the surface of spray-dried milk particles, which greatly exceeds the bulk fat content, is typically encountered independent of the atomization process. This surface dominance of fat causes detrimental effects on the powder particles' oxidative stability [24,25,27], affinity to caking [28,36] and dispersibility as well as wettability during reconstitution in water [16,35]. As a result, post-processing steps, such as coating with lecithin, are often used in industry for further processing and to prolong storage. Various potential mechanisms have been proposed to describe the component segregation mechanism between lipid, protein and lactose that leads to this fat accumulation at the surface during convective drying of milk droplets. Previously, it has often been attributed to the components' different physical properties that come into effect during the actual drying process subsequent to film disintegration. These include surface activity

[15,22,1], diffusivity [33,30,20,37] and solubility [5,29,49]. Yet, it was recently shown that it was, in fact, the atomization process that induces the fat surface coverage [18]. Immediately after atomization, the surfaces of milk model droplets were found to have fat contents of 9–13 and 83–92% v/v, respectively, for 0.5 and 44.2% v/v of fat on dry matter basis (d.m.) in the feed emulsions. In the subsequent drying stage, the layer of fat remained on the surface, while protein accumulated underneath the fat layer as drying proceeded. The comparison between atomized droplets and fully spray-dried particles was made possible by flash-freezing the atomized droplets. However, no information could be obtained on the droplet surface composition at intermediate drying times inside the drying tower. Moreover, the impact of the forming crust and of the corresponding surface composition on the drying and shrinkage kinetics of the droplets would be of great interest for optimization of industrial dryer design and operation.

In contrast to spray drying experiments, single droplet drying facilitates a direct monitoring of the convective drying of a solution or emulsion droplet at any point of the drying process [48,45]. The filament single droplet drying technique, where an individual droplet is suspended at a thin filament and dried in a conditioned air

* Corresponding author. Fax: +61 399055686.
    E-mail addresses: martin.foerster@monash.edu (M. Foerster), thomas.gengenbach@csiro.au (T. Gengenbach), meng.woo@monash.edu (M.W. Woo), cordelia.selomulya@monash.edu (C. Selomulya).

stream, has often been applied for this purpose, for instance the drying of aqueous droplets containing fruit pulp, milk and lactose [8,7,32]. Parameters such as relative air velocity, drying air humidity and temperature can be adjusted to observe the resulting changes in droplet mass, diameter and temperature in situ. Chen and Xie [9] introduced a semi-empirical model, the Reaction Engineering Approach (REA), to process this experimental data for description of the 'apparent activation energy of evaporation' as a measurement of the evaporation resistance of the emerging crust as a function of the droplet moisture content. Evaporation is hereby treated as an activation process that has to overcome a certain energy barrier. The single droplet drying technique does not allow for the complex droplet-droplet and droplet-air interactions encountered within spray dryers and the droplet size is significantly larger than in spray drying. It offers, however, a practical way of replicating the actual drying process of an individual droplet to determine the characteristic convective drying behaviour of a certain material system. This information can then be fed into computational fluid dynamics (CFD) simulations to predict the changes in moisture content and droplet size for the given material system in a spray dryer environment. In this way, the evaporation and shrinkage kinetics, even for complex solidification processes, are described with high accuracy [50,39,51]. Mezhericher et al. [34] proposed an incorporation of REA into a numerical model of the mass and temperature change in drying skim milk droplets for a more realistic account of the water diffusion resistance caused by crust formation. Chew et al. [12] undertook an investigation of the surface composition of fully dried milk protein concentrate particles subsequent to completion of the single droplet drying. The dried particles were analysed regarding to their chemical surface concentration via X-ray photoelectron spectroscopy (XPS), and it was found that smaller droplet sizes as well as higher temperatures resulted in a decreasing fat content on the particle surface, although there was always a significant overrepresentation of fat on the surface. Fu et al. [20] conducted a wetting and dissolution study of fresh whole and skim milk particles obtained from single droplet drying to qualitatively classify the surface as hydrophobic or hydrophilic. After certain drying times, the drying air flow was stopped and a solvent droplet (ethanol or water) was attached to the (semi-)dried droplet. Based on the wetting behaviour observed with a camera, conclusions about the nature of the developed surfaces were drawn. Interpretation, however, was limited to a relative comparison between whole and skim milk, and the wettability until about 35 s from drying commencement could not be studied because of too high moisture contents.

In order to gain a better understanding of the material segregation process that occurs in a convective drying of milk droplets, the final surface concentration alone or ambiguous dissolution test videos are insufficient. To date, single droplet drying has not yet been applied for quantitative analysis of the surface composition at intermediate drying stages and directly after droplet generation. The aim of the present study was to widen the hitherto employed extent of single droplet drying analyses to also monitor, for the first time, the changes in surface composition and internal component distribution over drying time and over the corresponding droplet moisture content. Single droplet drying of low and high fat milk model emulsions was interrupted at discrete drying times by cryogenic flash freezing, and, following freeze-drying, the particles were analysed in terms of surface composition by XPS and internal

component distribution by confocal laser scanning microscopy (CLSM). The data were compared with drying and shrinkage kinetics obtained from conventional single droplet drying experiments for a better understanding of surface formation and its impact on the convective drying behaviour of milk droplets. A requirement for these results to be representative for the surface composition and drying characteristics in a spray dryer was that the initial droplet states were comparable. It was hence to be validated that the component distribution in the droplets generated for single droplet drying matched the one of droplets atomized during conventional spray drying.

2. Material and methods

2.1. Emulsion preparation

Two model milk emulsions of different fat contents were investigated, as summarized in Table 1. A fat filled model emulsion (FFME) featured a composition typical for both bovine whole milk and commercially sold fat filled milk powder. It contained 40.8% w/w lactose, 31.1% w/w fat and 27.0% w/w protein in d.m. A low fat model emulsion (LFME) resembled the composition of the FFME in terms of protein-lactose ratio and solid content, whereas the fat content was significantly reduced to 0.3% w/w. The emulsions were prepared by dissolving α-lactose monohydrate (Sigma-Aldrich Co., USA), calcium caseinate isolate (Nutrients Direct Pty Ltd, Australia) and whey protein isolate (Nexius Pty Ltd, Australia) with a caseinate/whey ratio of 4:1 in water. For the FFME emulsion, sustainably sourced refined *Elaeis guineensis* palm oil fat (Auroma Pty Ltd, Australia) was added. Both emulsions were mixed with deionised water at 45 °C for 1 h, prior to pre-homogenization in a high-speed colloidal mill (WiseMix Homogenizer HG-15D, Daihan Scientific, South Korea) at 1000 rpm. This was followed by three passes at 1000 bar and two subsequent passes at 500 bar through a high pressure homogeniser (EmulsiFlex-C5, Avestin, Canada). The fat globule size distributions of each emulsion were measured by dynamic light scattering (Zetasizer Nano ZS, Malvern Instruments Ltd, UK) to ensure consistency (volume weighted mean diameter had to be $D[4, 3] = 1.0 \, \mu m \pm 0.05 \, \mu m$).

2.2. Changes in component distribution over drying time via cryogenic flash-freezing

Information about changes in the internal and surface distribution of lactose, protein and fat with proceeding drying time was acquired from single droplet drying experiments conducted inside a suspension rig with well-defined drying environment. Compressed air flowed through a dehumidifying column (KF-DDF-125, Knight Pneumatics, Australia) and was electrically heated before entering the drying chamber from the bottom and leaving it through its top. The conditioned air stream had a temperature of 70 °C, a velocity of 0.75 m/s and a humidity of 0.0001 kg/kg. Individual FFME and LFME droplets of 3 μl (±0.05 μl standard deviation) were generated by means of a 5 μl micro-volume syringe (5FX, SGE Analytical Science, Australia) and were then suspended at the tip of a thin, vertically mounted glass filament. The tip of the filament consisted of a knob which had a hydrophilic coating

Table 1
Volumetric composition of the solid contents in the LFME and FFME model emulsions.

	Abbreviation	Solid concentration [% w/w]	Fat content in d.m. [% v/v]	Protein content in d.m. [% v/v]	Lactose content in d.m. [% v/v]
Low fat model emulsion	LFME	20.0	0.5	41.8	57.7
Fat filled model emulsion	FFME	20.0	44.2	23.5	32.4

at its lower half and a hydrophobic one at its upper half. The beginning of the drying process was controlled with a by-pass slider separating the chamber from the air stream. The drying process was stopped abruptly after certain drying times to virtually freeze the component distribution. At 0, 20, 50, 100 and 200 s, the drying droplets were flash-frozen directly inside the drying chamber by immersing them in cryogenic vials that were filled with liquid nitrogen and that were raised from the chamber bottom up towards the droplet (Fig. 1a). The frozen droplets were then immediately taken out of the drying chamber together with their glass filament by pulling the filaments down from the filament holder, to which they had been connected loosely with adhesive tape. For a drying time of 0 s, the generated droplets were directly immersed from the syringe into liquid nitrogen. The flash-frozen droplets were stored in the liquid nitrogen filled vials, which were kept sufficiently cool by dry ice, until freeze drying. The freeze drying was performed with a FreeZone 2.5 l benchtop freeze dry system (Labconco Corp., USA) at −80 °C and 0.1 mbar for 24 h. The component distribution of particles dried for 420 s was also analysed, but did not require flash-freezing, because the drying process of those particle was already completed. All of these singe droplet drying runs were performed in duplicate.

2.3. Spectroscopic surface composition analysis

XPS was employed to analyse the chemical surface compositions of the flash-frozen and fully dried particles of both model emulsions. Analyses were performed either on an AXIS Ultra DLD or an AXIS Nova (Kratos Analytical Inc., UK), both spectrometers equipped with a monochromated Al K_α source, a hemispherical analyser operating in the fixed analyser transmission mode and using the standard aperture (analysis area of 0.3 mm × 0.7 mm). The particles were mounted on custom-built sample holders by taping their glass filaments to the holder so that the particles themselves remained suspended in space, without coming into contact with the holder. Each particle was analysed at a nominal photoelectron emission angle of 0° with respect to the surface

normal. As the actual emission angle is ambiguous in the case of particles, varying between 0° and 90°, the sampling depth would vary between 0 nm and approximately 10 nm. The pressure in the main vacuum chamber during analysis was of the order of 10^{-8} mbar. All detected elements were identified from survey spectra. Their relative atomic concentrations were computed from the integral peak intensities and the sensitivity factors provided by the manufacturer. The concentrations in lactose, fat and protein can be assumed to be linear combinations of the atomic surface composition [17]. The fraction of each component at the surface, expressed in atomic concentrations, was hence estimated by linearization based on the representative structural formulas of lactose, milk fat and milk protein, as elaborated elsewhere [12].

2.4. Confocal laser scanning microscopy

The protein and fat distribution in flash-frozen as well as fully dried FFME particles were analysed via CLSM. Based on the procedure described by Taneja et al. [47], dual labelling with fluorescent dyes was performed during emulsion preparation. The molten fat and the reconstituted protein powder were stained with 0.02% w/w hydrophobic Nile Red and 0.01% w/w hydrophilic Fast Green FCF, respectively (Sigma Aldrich Co., USA). Similar to the above described procedure, the constituents were then mixed and the emulsion was homogenized. The labelled droplets were subsequently dried in the single droplet drying rig for discrete drying times, followed by freeze drying to remove the remaining moisture, if applicable. The resulting particles were mounted on a microscope slide with DPX (Sigma Aldrich Co., USA) and investigated by CLSM with a Nikon A1$^+$ confocal microscope (Nikon Corp., Japan). Nile Red, attached to the fat, and Fast Green FCF, attached to the protein, were sequentially excited by respective laser lights from a helium–neon (637 nm) and an argon (487 nm) source. The images were taken through a 4× magnification lens with a resolution of 2048 × 2048 pixels in the x-y plane at different z-depths inside the particles.
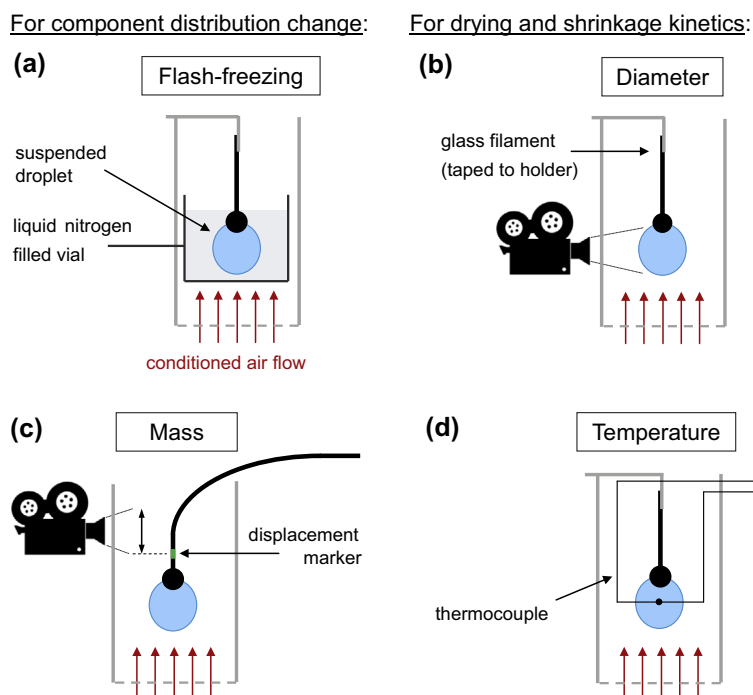

Fig. 1. Schematic illustration of the experimental single droplet drying set-ups: (a) component distribution analysis; (b) diameter change analysis; (c) mass change analysis; (d) temperature change analysis.

2.5. Change in droplet diameter, mass and temperature over drying time

In addition to the component distribution study, single droplet drying was also conducted in the conventional way to obtain information about the temperature, mass and diameter profiles of the model milk droplets. The experimental procedure followed the methodology described by Fu et al. [21], and a schematic illustration is given in Fig. 1b–d. In brief, droplets with an initial volume of 1, 2 or 3 μl were generated and attached to vertical glass filaments inside the drying chamber, similar to the above described procedure. In this case, however, the drying process was not interrupted by flash-freezing. Instead, in-situ analyses were conducted simultaneously to the drying process. The profiles of droplet diameter, mass and temperature changes were obtained from separate single droplet drying runs. Firstly, as illustrated in Fig. 1b, the projected droplet areas were recorded with a camcorder (DCR-HC36, Sony Corp., Japan) equipped with five 4× close-up lenses (Marumi Optical Co. Ltd., Japan) to estimate the droplet volume and thus the equivalent droplet diameter over time. Secondly, the changes in droplet mass during drying were monitored by attaching the droplets at the tip of an elastic glass filament (Fig. 1c). The displacement of a marker at the filament was recorded with the camera and the correlating mass change was derived from a previously performed calibration with standard weights consisting of agglomerated glass beads. Thirdly, changes in temperature over drying time were measured by inserting a type K thermocouple (Omega Engineering Inc., USA), which was attached to a Picolog USB TC-08 data logger (Pico Technology, United Kingdom), into the droplets (Fig. 1d). The videos of the droplet diameter and mass change analyses were rendered into a sequence of individual images with Blender 2.69 (Stichting Blender Foundation, The Netherlands) and processed using ImageJ 1.48 (National Institutes of Health, USA). Each of these single droplet drying runs was run in triplicate. The obtained data was processed according to the hereafter described REA methodology.

2.6. Drying and shrinkage kinetics from single droplet drying data

Data about the changes in droplet diameter, mass and temperature, which had been obtained from single droplet drying experiments as described above, was processed according to the Reaction Engineering Approach. The REA describes convection drying as a result of differences in the vapour density between drying air and droplet surface, as will be briefly described in the following and outlined in detail elsewhere [9]. The drying rate dm_w/dt as loss in water content m_w over time t was calculated by

$$dm_w/dt = -h_m * A * (\rho_{v,s} - \rho_{v,b}) \tag{1}$$

where h_m was the convective mass transfer coefficient, A the surface area of the droplet, and $\rho_{v,s}$ and $\rho_{v,b}$ the vapour density at the droplet surface and of the bulk air, respectively. The convective mass transfer coefficient was computed with a modified Ranz-Marshall correlation [41,42,31], which is well suited for high vapour fluxes as they occur in single droplet drying. The surface vapour density changed with drying time, and was correlated with the saturated surface vapour density $\rho_{v,sat}$ by means of the fractionality coefficient ψ

$$\rho_{v,s} = \psi * \rho_{v,sat}(T_s) \tag{2}$$

where T_s was the temperature at the interface. The fractionality coefficient depended on the activation energy ΔE_v, as described by the following formulation of an Arrhenius equation:

$$\psi = \exp\{-\Delta E_v/(R * T_d)\} = -R * T_d * \ln(\rho_{v,s}/\rho_{v,sat}(T_d)) \tag{3}$$

where R was the universal gas constant. Since the Biot number lies well below unity in single droplet drying applications [38], the temperature gradient inside the droplet could be neglected and the surface temperature could be approximated with the internal droplet temperature T_d. The apparent activation energy reflected the vapour concentration depression at the interface of the droplet as a result of a reduction in free surface water due to influences such as component precipitation and crust formation. Eqs. (2) and (3) substituted into Eq. (1) lead to the following expression of the drying rate:

$$dm_w/dt = -h_m * A * [\rho_{v,sat} * \exp\{-\Delta E_v/(R * T_d)\} - \rho_{v,b}] \tag{4}$$

For a given convective drying condition, the drying rate can hence be predicted if the apparent activation energy is known as a function of droplet moisture content. This correlation was determined via single droplet drying experiments by recording the changes in droplet mass, droplet temperature and droplet surface area, as rearrangement of Eq. (4) shows:

$$\Delta E_v = -R * T_d * \ln[(-(dm_w/dt) * (1/(h_m * A)) + \rho_{v,b})/\rho_{v,sat}] \tag{5}$$

The experimentally established apparent activation energy over droplet moisture content was described in normalized form by its maximum value $\Delta E_{v,max}$, which eventuated when the vapour densities at the surface and in the bulk air reached equilibrium:

$$\Delta E_{v,max} = -R * T_b * \ln(\rho_{v,b}/\rho_{v,sat}(T_b)) \tag{6}$$

The normalized activation energy over the free moisture content $(X - X_e)$ of the overall droplet volume was to be described in the following form:

$$\Delta E_v/\Delta E_{v,max} = a * \exp\{b * (X - X_e)^c - 1\} + 1 \tag{7}$$

where X was the absolute moisture content and X_e the equilibrium moisture content. The latter one was found via the Guggenheim–Anderson–de Boer desorption isotherm following Chen and Lin [7]. In addition, an empirical relationship for the normalized droplet diameter was determined from the same single droplet drying experiments:

$$D/D_0 = A + (1 - A) * (X - X_e)/X_0 \tag{8}$$

where X_0 was the initial moisture content. In the first approximation, linear correlations usually describe the droplet shrinkage with sufficient accuracy for food drying applications [40].

3. Results and discussion

3.1. Qualitative distribution of fat and protein in the particles

Fig. 2 illustrates the qualitative fat and protein distribution in drying FFME droplets of 3 μl initial volume by taking the example of a fully dried FFME particle. The component distributions after an earlier interruption of the drying process were found to be similar to the one presented here in case of the FFME emulsion. The fat and the protein of the FFME emulsion could be stained individually prior to mixing of both phases, and thus the two components were clearly distinguishable in the CLSM analysis. Yet, the image quality of the LFME particles was not satisfying, since the fat phase could not be visualized. The fat content of the LFME emulsion originated directly from the protein isolates and thus the fat globules were not available in isolated form without a surounding protein membrane, which inhibited penetration by the Nile Red stain. In Fig. 2, the response channels obtained from sequential excitation of the FFME particle were superimposed. The signal emmited from Nile Red, being attached to the lipid phase, is depicted as brownish red and the signal from Fast Green FCF, which attached to the protein, is represented in green colour. Areas of relatively high concentrations in both protein and fat appear yellow. 60 high resolution
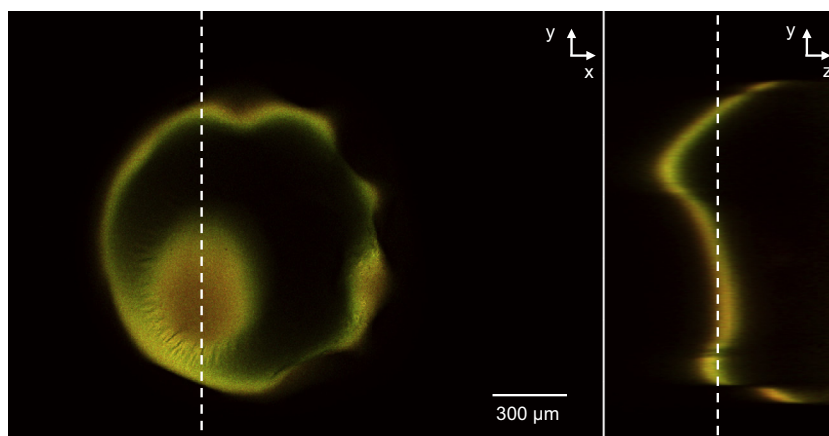
Fig. 2. Fat and protein distribution in a FFME particle after completed single droplet drying (420 s) as obtained by CLSM: two cross-sections through the three-dimensional image stack as indicated by the dotted lines, Nile Red (fat dye) and Fast Green FCF (protein dye) are depicted in red and in green, respectively. (For interpretation of the references to color in this figure legend, the reader is referred to the web version of this article.)

images were taken at a step size of 35 μm from the very particle surface towards the inner of the particle at a location far away from the contact point of the glass filament. From both the *x-y* and the *z-y* plane, it can be seen that the outermost particle surface was dominated by fat, as a consistent fat film encased the whole particle. The pixel size of the CLSM images was 1.6 μm, and hence in the same order of magnitude than the individual fat globules present in the emulsions. The existence of a fat film rather than individual lipid islands suggested that, in case of the FFME, the globules were ruptured by mechanical stress during the droplet generation process and thus spread over the whole droplet surface. Directly underneath the fat surface film, there was generally a high accumulation of protein. With an average of about 30–60 μm, the radial thickness of the transition region from the surface fat film to protein domination was very thin in relation to the total droplet and particle radii (approximately 600–800 μm).

Below the outer fat film and the subjacent protein, no fluorescent signal was received from the inside of the particles (large black internal space in Fig. 2). Theoretically, this could mean that that region was completely free of fat and protein, being filled with lactose and/or voids only. However, it was calculated by simple mass balance that the volume of the 'surface shell' that was visible in the CLSM images accounted for only about 30–35% of the total fat and protein volume contained in a 3 μl FFME droplet. Also, scanning electron microscopic analysis of sliced particles (not shown here) showed that the particle centres did not consist of any significant voids or hollows, but the whole particle matrix was interspersed with a network of small pores due to the freeze-drying step. Therefore, it was concluded that at a certain radial depth the exciting laser light and the emitted fluorescent signal had become too weak to produce a detectable response. Limited penetration depths due to low signal strength is a typical problem in conventional confocal microscopy, since scattered light is not detected by the spatial pinhole [26]. Accordingly, as can be seen in the *z-y* plane of Fig. 2 by the thinning 'surface shell' with increasing depth, the flourescent response signal became weaker in *z*-direction with increasing distance from the instrument's laser source and detector until vanishing completely. In the *x-y* plane, this effect was enhanced by the relatively low protein and fat concentrations in the inside of the particles. Since there was an overrepresentation of these components neat the surface, it is realistic to consequently assume a stochiometric overrepresentation of lactose in the particle middle.

Despite the different size scale and generation technique of the droplets, the existence of a surface fat layer with adjacent protein accumulation agrees well with the analysis of the CLSM images of spray-dried milk particles and their corresponding freshly atomized droplets from a microfluidic multi-jet spray dryer [18]. For detailed discussion of the potential reasons for the observed component segregation mechanism that occurred during the single droplet drying process, the quantative surface composition analysis via XPS needs to be taken into account.

3.2. Chemical surface composition of the high-fat emulsion droplets at discrete drying times

Fig. 3 illustrates the surface composition of the drying FFME and LFME droplets, obtained from XPS analysis, as a function of the free moisture content $(X - X_e)$. Defined as total water content over total solid content in kg/kg, the moisture content X was calculated from the experimentally obtained mass change data. It decreased from 4 kg/kg until approximating the calculated equilibrium moisture content, and the equilibrium moisture content was taken as the final moisture content. In addition, also the corresponding drying time is given for each analysis point. After 7 min the droplets were fully dried and could be directly analysed, whereas for any shorter drying time (0, 20, 50, 100 and 200 s) the droplets were flash-frozen and subsequently freeze-dried prior to XPS. The standard deviations in the relative atomic concentrations were relatively small and are depicted in Fig. 3. The absolute values in lactose, protein and fat surface concentration should nonetheless be treated as estimates only, because some uncertainty might have been introduced by the linearization step.

Most notably was for the FFME droplets that their surface consisted almost exclusively of fat (Fig. 3a). The fat accounted for a concentration of 90 to nearly 100% v/v throughout the whole drying process, which was more than double as high as the overall fat concentration in the emulsion. This corresponds well with the CLSM observation of a consistent fat film, which appeared thicker than the maximum XPS sampling depth of approximately 10 nm. The fat concentration did not reach a total 100% v/v, however, owing to small amounts of protein. These presumably had been part of the protein membrane around the fat globules in the emulsion and hence became entrapped inside the fat surface film. The fat is believed to have already emerged at the droplet surface at the time of droplet generation, as the initial fat concentration of 92.6% v/v fat indicates. Due to its hydrophobicity, the lipid phase accumulated at the droplet surface while the droplet was formed with the micro-volume syringe. Transport to the surface might have occurred by means of convection currents and circulation
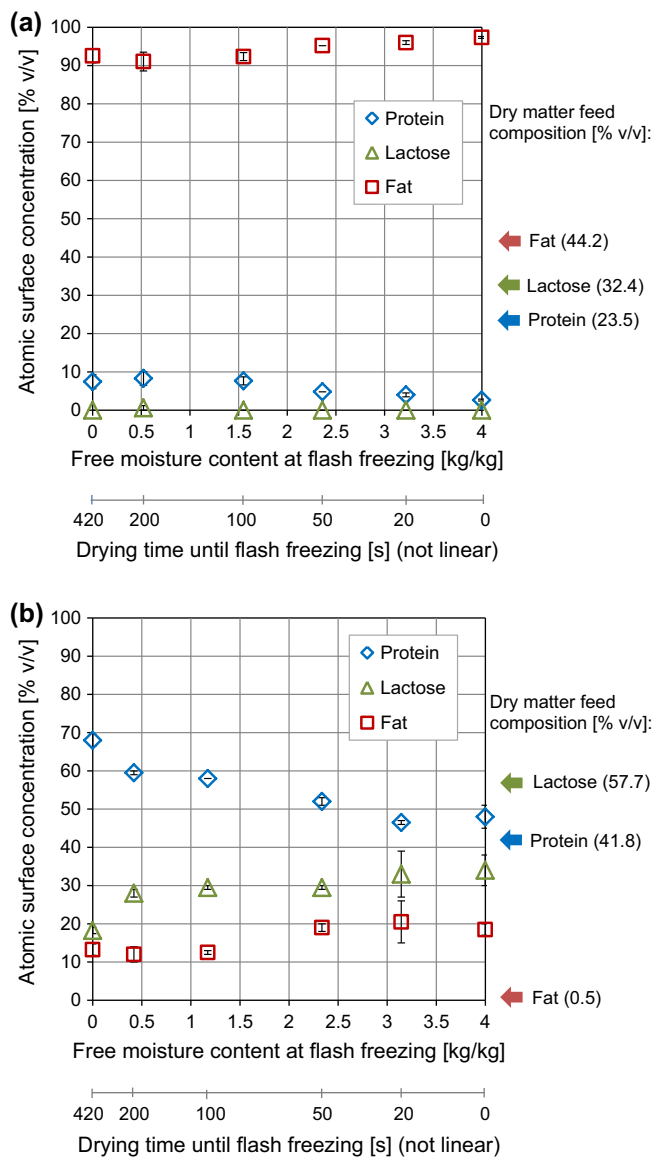
Fig. 3. XPS particle surface composition in protein, lactose and fat for certain drying times and the corresponding free moisture contents, in comparison with the overall dry matter compositions of the feed emulsions: (a) FFME droplets; (b) LFME droplets. Droplets were flash-frozen and freeze-dried prior to analysis for drying times of 0–200 s.

inside the droplet upon its generation. It is interesting that a similar atomization induced fat surface accumulation has also been reported in [18], although the droplets were generated with a microfluidic jet nozzle, a pressure swirl nozzle and a rotary disc nozzle and their size was substantially smaller. Further study of the droplet formation process will be required in order to better understand the underlying mechanisms that led to the observed initial surface composition independent of the type of film disintegration. In the case of 0 s drying time, approximately two to three

seconds elapsed until the droplet was immersed in liquid nitrogen following the droplet generation. Droplet generation typically took about one to two seconds. This duration was most likely not sufficient to allow a considerable amount of fat globules to travel towards the droplet surface by diffusion, given their relatively slow diffusivity at room temperature as shown in Table 2. The presented diffusion time scales τ_i of each component i over a diffusion length l of 50 μm were approximated with the aid of binary diffusion coefficients D_i, which were calculated with the Stokes-Einstein's equation [14]:

$$\tau_i = l^2 / D_i \tag{9}$$

$$D_i = K_B T / (6\pi \mu R_i) \tag{10}$$

where K_B was the Boltzmann's constant, T the temperature, R_i the component radius, and μ the dynamic viscosity of water. The resulting values only represent qualitative comparison of the relative diffusivities between fat globules, protein and lactose. The absolute values must be treated with caution, considering the uncertainty about the exact diameter of the species during drying and the very limited validity of the Stoke-Einstein's equation, particularly an infinite dilution assumption.

In the drying process subsequent to droplet generation, the droplet surface remained covered by the fat film due to its hydrophobicity. There was, however, a trend of increasing protein content at the surface from 4.4 to 7.5% v/v.

3.3. Chemical surface composition of the low-fat emulsion droplets at discrete drying times

The investigation of the LFME behaviour during single droplet drying (Fig. 3b) gave a better insight into the protein migration process. Also in this case the fat was highly overrepresented at the surface in comparison to the bulk composition. With a fat concentration of 0.5% v/v in d.m. in the feed emulsion, a multiple thereof was present at the droplet surface, starting with 18.5% v/v and then declining marginally to approximately 13.5% v/v. However, this time the fat did not dominate at the surface. Again, the surface compositions of the droplets generated with the micro-volume syringe were similar to droplets of the same milk model emulsion after atomization in different spray dryers as reported by Foerster et al. [18]. Consequently, the observed surface formation and drying kinetics could be considered as representative for droplets in a spray dryer. On a general note, however, such an agreement in initial droplet surface state between single droplet drying and spray drying is not guaranteed, because the droplet generation process in single droplet drying is different to the disintegration mechanism in an atomization nozzle. This hence needs to be validated case-by-case. Due to the lower fat content at the surface in comparison to the FFME droplets, a significant rise in protein surface concentration with proceeding drying time could be observed. This protein migration to the surface was presumably governed by diffusion, since the diffusion time of the caseinate molecules possibly lay within the range of the singe droplet drying time scale (Table 2). The cause of this diffusion could have been twofold. First, the drying process induced a radial gradient in water

Table 2
Binary diffusion coefficients of fat globules, caseinate and lactose in water at infinite dilution from Eq. (10) together with the corresponding diffusion time scales for a length of 50 μm from Eq. (9). The radii were determined by dynamic light scattering for fat and protein and taken from Bylund [4] for lactose.

	Mean radius [nm]	Diffusivity [m²/s]		Diffusion time scale [s]	
		At 25 °C	At 50 °C	At 25 °C	At 50 °C
Fat globules	1000	$2.2 \cdot 10^{-13}$	$1.2 \cdot 10^{-12}$	5724	1056
Protein (caseinate)	75	$2.9 \cdot 10^{-12}$	$1.6 \cdot 10^{-11}$	429	79
Lactose	0.5	$4.4 \cdot 10^{-10}$	$2.4 \cdot 10^{-09}$	2.9	0.53

concentration from the inner of the droplet towards the surface, where water was continuously removed as a result of evaporation. Consequently, concentration gradients in fat, lactose and protein developed in reverse direction from the surface towards the droplet centre and induced diffusion towards the centre. As there was a considerable difference in the diffusivities of the components (Table 2), they diffused at dissimilar speeds. The diffusivity of lactose exceeded the one of caseinate by about two orders of magnitude. This might have led to enrichment of protein, in comparison to the lactose concentration, at the outer droplet regions. Second, caseinate molecules are surface active and therefore a part of them could adsorb at the air-water interface of the droplets [23]. As such, this adsorption at the surface reduced the concentration gradient in free diffusing protein molecules and thus counteracted the above described protein movement towards the droplet centre.

While an efficient encapsulation of the fat phase in the particle middle is desired in industrial applications for optimum functional properties, high amounts of protein at the particle surface can also imply detrimental effects. For instance, it has been shown that native casein micelles are prone to form an interlinked network between the surfaces of aggregated powders, hence reducing the dispersibility and water penetration ability [46,13]. Fig. 3 b further shows that, concomitant with the increase in protein concentration, the lactose surface concentration declined from 34.0 to 18.3% v/v. The comparatively low lactose surface content potentially influenced the particles' solubility in aqueous medium adversely [2,3].

Although the diffusivity of the fat globules was even about one order of magnitude smaller than the one of caseinate, the surface of the LFME droplets did not further enrich in fat over drying time. The reason for this might be that the high protein-to-fat ratio in the low-fat emulsion, in combination with the low fat globule size of 1 µm in diameter, lead to an extensive encapsulation of the fat globules by thick protein membranes that were bound to them. Thus, despite a potential concentration of the slow diffusing fat globules at the droplet surface, the surface fat content did not exceed a certain threshold. The comprehensive protein membranes were also believed to prevent rupture of the fat globules and consequent spreading of a consistent fat film over the droplet surface, unlike the observations made for the FFME droplets.

The results of this modified single droplet drying technique were compared with the study conducted by Fu et al. [20], where the same single droplet drying rig at identical drying air temperature and flow rate was used for 2 µl skim and whole milk droplets. In agreement with the results discussed in respect to Figs. 2 and 3, after a drying time of 50–80 s both investigated emulsions featured semi-dried droplets with hydrophobic shells, which were less water-wettable for whole milk in comparison to skim milk. Yet, they concluded an increasing surface fat content with drying time from a rise in repulsion of attached water droplets, which does not correspond with the outcomes of this study. The wettability might have been impaired by a proceeding crust formation rather than by a supposed increase in fat content on the surface of that crust. Interpretation of the dissolution study were ambiguous due to overlapping influences between different rates of crust formation for whole and skim milk and the actual difference in composition between those crusts. In conclusion, the advantage of the proposed single droplet drying technique over such a dissolution study seems to be that it allows to, firstly, investigate droplets immediately subsequent to their generation at any moisture content and, secondly, to observe the change in the components' surface concentration itself.

3.4. Changes in droplet mass, temperature and size

How the observed changes in component distribution near the surface of drying FFME and LFME droplets influenced their drying and shrinkage characteristics was evaluated on the basis of the other single droplet drying measurements. Excerpts of the corresponding data about the droplet mass, temperature and diameter behaviour over drying time are shown in Fig. 4. The evaporation rate was identified to be considerably faster in the early drying stage (Fig. 4a and b). The curve shapes agreed well with mass change data from literature for 20% w/w skim milk droplets of 1.6 µl initial volume at 91.4 °C drying air temperature [7]. The final particle masses were proportional to the initial droplet volumes. The mass changes at early drying were most rapid, as with proceeding drying the crust formation built up an increasing mass transfer resistance for moisture movement towards the surface. This was also reflected in the horizontal axes of Fig. 3: for instance, the free moisture content of the 3 µl FFME droplets had been reduced from 4.0 to 1.55 kg/kg after the initial 100 s of drying, whereas it only altered by about 1.0 kg/kg to 0.52 kg/kg in the following 100 s. In comparison, during the first 100 s of drying of the 3 µl LFME droplets, the free moisture content sank more significantly to 1.17 kg/kg. This indicated that a lower fat content (at equal total solid content) favoured water transport to the surface and hence evaporation from the surface.

It can be seen from Fig. 4c and d that the temperature profiles approached asymptotically the bulk temperature of the drying air (70 °C). Slight dips in the temperature rise took place at the wet bulb temperature of approximately 25–30 °C after 15–40 s drying time. There were no distinct temperature plateaus as for example found during the single droplet drying of lactose solutions by Fu [19], since lactose is not shell forming and thus allowed free surface water throughout most of the drying process. The immediate formation of a hydrophobic fat film on the surfaces of both model emulsions presumably further contributed to the very low free surface water and the consequent lack of a temperature plateau at wet bulb temperature.

The observed profiles of the normalized droplet diameters over drying time (Fig. 4e and f) corresponded well with the results obtained by Chew et al. [11], where skim milk droplets of 40% w/w initial solid content were investigated in the same single droplet drying rig at various drying air conditions. Yet, the shrinkage was less pronounced in the experiments conducted by Chew et al. [11] due to a higher solid content. The bigger the initial droplet volume was, the longer was the existence of an appreciable change in diameter and the larger was the final normalized diameter of the dried particle. For larger initial droplets, it is believed that full crusts at the surface had been developed earlier relative to the remaining total amount of moisture inside the droplets. These solidified shells decelerated the moisture transport to the droplet surfaces and inhibited the degree of shrinkage relative to the initial diameter. Furthermore, comparison between Fig. 4e and f revealed that more considerable shrinkage occurred for a lower fat content. In consideration of that, the fat content seemed to also have a significant influence on the shrinkage kinetics and the final particle size, as will be discussed in the following in respect to the REA outcomes.

3.5. Shrinkage kinetics

The temperature, mass and diameter data were processed by means of the Reaction Engineering Approach to produce correlations between the normalized diameter and the free moisture content as well as between the normalized activation energy of evaporation and the free moisture content. As can be seen in Fig. 5a, the normalized diameter curves for the different initial droplet sizes of FFME lied close together and featured a proportional relationship between normalized diameter and free moisture content. The r^2 value and the fitting parameter A of the corresponding linear trend line, which was expressed in accordance to Eq. (8), are
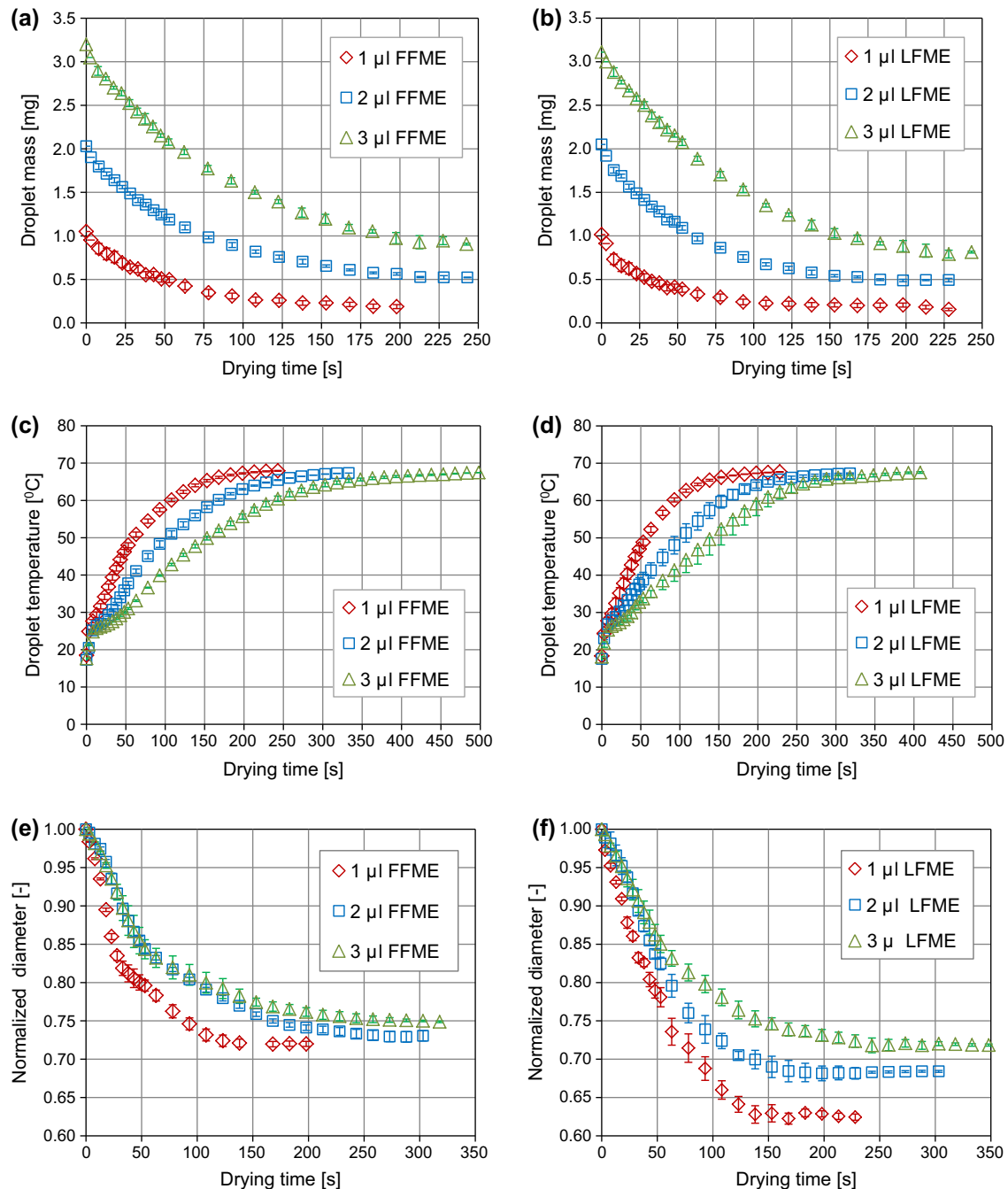
Fig. 4. Experimental results from single droplet drying for FFME and LFME droplets with different initial volumes over drying time: (a), (b) droplet mass; (c), (d) droplet temperature; (e), (f) normalized droplet diameter.

given in Table 3. In contrast, the normalized diameter curves of the LFME droplets varied appreciably with their initial volumes of 1, 2 and 3 µl, as reflected by the considerably lower r^2 value of the linear fitting curve of all LFME points. In particular once the moisture contents came below 0.5 kg/kg, the curves of the different initial LFME droplet sizes deviated significantly. For the smallest initial size, the droplets experienced a significant further shrinkage at low moisture content, whilst the diameter hardly changed anymore for droplets with an initial volume of 2 and 3 µl. This was in agreement with a study conducted by Chew et al. [10], where out of three milk model emulsions the one with the highest fat content featured the least shrinkage, particularly at low moisture content. In addition, also at intermediate moisture contents (3.5–1 kg/kg) the normalized diameter curves described different

trends, in particular comparing the drying droplets of 1 and 3 µl initial volume.

Comparing the normalized diameter profiles of the two model emulsions, the low-fat droplets experienced more shrinkage relative to the initial diameter owing to a more significant decrease in diameter in the second drying half (2.0–0 kg/kg free moisture content). All these described differences in the normalized diameter curves for different initial droplet sizes (in case of the LFME emulsion) and for different fat contents were clearly greater than the depicted standard deviations. It was therefore concluded that the different fat contents and the surface composition of the drying droplets exerted crucial impact on the shrinkage characteristics. As a result of water evaporation from the surface, the droplets became enriched in their non-aqueous components near the surface with
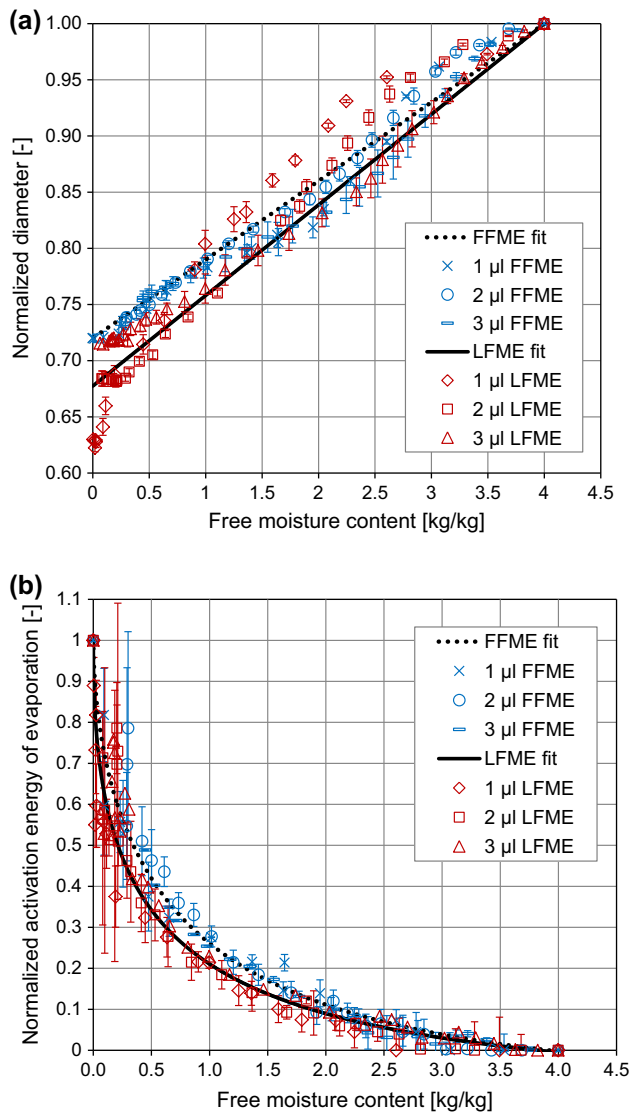
Fig. 5. From single droplet drying experiments derived drying and shrinkage kinetics for FFME and LFME droplets with different initial volumes over free moisture content, including one trend line fittings for all volumes each and propagated error bars: (a) normalized droplet diameter; (b) normalized activation energy of evaporation.

Table 3
Correlations of the normalized activation energy of evaporation and the normalized droplet diameter over free moisture content: fitting constants *a*, *b*, *c*, *A* and coefficients of determination r^2 with regard to Eqs. (7) and (8), respectively.

	Norm. activation energy				Norm. diameter	
	a	*b*	*c*	r^2	*A*	r^2
FFME	1.092	−1.130	0.575	0.952	0.720	0.962
LFME	1.104	−1.256	0.471	0.951	0.677	0.700

an increase in water concentration towards the centre. The FFME droplets were covered by a fat film throughout the whole drying process. Consequently, the crust that was forming in the surface region featured hydrophobic properties and, as such, inhibited shrinkage of the drying droplet due to repulsion towards the moisture in the droplet centre. In comparison, the shells of the LFME droplets underwent more contraction, because they did not contain a dominating amount of fat in their peripheral areas. Instead, 48–68% v/v of the surface was occupied by protein (Fig. 3b).

Because of attractive forces between the hydrophilic groups of the protein and the water contained inside the droplets, the surface shell presumably was less resistive to further changes in diameter in comparison to the FFME droplets. The complex impact of various kinds of protein on the shell behaviour in drying droplets is an area of high interest for various applications. The physical properties, such as sol-gel transition, molecular weight and conformation behaviour, can vary widely, even for the different protein types encountered in milk. For instance, native casein micelles tend to arrange in soft, flexible shells. In contrast, whey protein has been shown to form hard, brittle shells with higher restraint to deformation at high concentration regimes [43,44]. In the present study, the protein component consisted to 80% w/w of calcium caseinate and to only 20% w/w of whey protein. As such, the protein shell of the LFME droplets was relatively flexible. Though caseinate molecules do not assemble in micelle structures like native casein, they feature strong hydration ability and a dynamic molecule structure, in particular in comparison to the denser, hydrophobic fat phase. In view of that, it is proposed that with advancing solidification at the droplet surface, the caseinate molecules were able to pack into a denser configuration under dehydration and reconfiguration. As a result, the shells of the LFME droplets, which were high in caseinate, remained more deformable than the high-fat content shells and exhibited a plastic behaviour at low moisture contents. Accordingly, despite ongoing solidification with longer drying time, the shell of the LFME droplets still possessed relatively high water permeability and flexibility in terms of shrinkage at low moisture contents, as the protein surface content was rising simultaneously (for instance from 59.5% v/v at a moisture content of 0.42 kg/kg to 68% v/v at completed drying). This could have allowed the above described considerable extent of shrinkage at a late drying stage. Possibly, a less rigid shell was also responsible for the LFME droplets being more prone to shell expansion and collapse as subject to vapour pressure in the droplet centre (if internal evaporation occurred) and capillary force. This is believed to have led to the above described, distinct deviations in the normalized diameter curves for 1, 2 and 3 µl initial droplet volume. For example, the rise in protein surface concentration might have been more pronounced for a shorter diffusion length and hence the normalized diameter curve of the 1 µl LFME droplets showed a stronger deviation from linear behaviour in comparison to the 2 µl and 3 µl LFME droplets.

3.6. Drying kinetics via reaction engineering approach

The activation energy of evaporation was calculated as a function of moisture content according Eq. (5) and its maximum value $\Delta E_{v,max}$ was determined by Eq. (6) in order to plot Fig. 5b. The standard deviations of the normalized activation energy points were reasonably low, except from the low moisture content region below 0.5 kg/kg. At slow evaporation rates the mass changes tended to go towards zero and so, along with a significant standard deviation in mass change relative to the absolute mass change, the propagated error in activation energy became large in this region. The normalized activation energy of evaporation increased exponentially with smaller free moisture content for both model emulsions. The reason for this was a rise in the apparent resistance to evaporation, as the vapour pressure at the droplet surface and the effective water diffusivity declined the more the further the crust formation had been advanced. Therefore, the water movement to the surface and the evaporation rate decelerated with preceding drying. Furthermore, the activation energy of the FFME droplets was slightly higher than the one of the LFME droplets at moisture contents of around 2.0 kg/kg and below. Because of the previously discussed hydrophobic character of the fatty surface shell that occurred in the FFME droplets, the water movement to

the droplet surface was additionally repelled in the drying FFME droplets. Whereas the shell of the FFME droplets was dominated by lipids throughout the whole single droplet drying process, the shell of the LFME droplets contained less than a quarter of this fat amount and protein enriched more and more with declining moisture content. In view of that, it was concluded that the higher fat content slowed down the drying process and concurrently limited the particle shrinkage. The obtained activation energy data did not scatter significantly between the different initial droplet volumes, and thus one trend curve for all FFME and another trend curve for all LFME points could be applied (r^2 value of 0.952 and 0.951, respectively). The mathematical expression of the trend curves followed Eq. (7), and the fitting parameters are presented in Table 3. This agreed with the results from previous studies of a range of solutions and emulsions with initial solid contents below 40% w/w, where the normalized activation energy curves were also approximately independent from the initial droplet volume [6,21]. In industry, such correlations for the activation energy of evaporation and droplet diameter can be implemented into CFD simulations to optimise process conditions, and to predict the moisture content and particle size of resulting powders, in response to fluctuations in the feed properties. In combination with component distribution data obtained from the modified single droplet drying analysis, the approach should allow a better understanding of a range of process conditions to control functional powder properties, such as stickiness.

4. Conclusions

The drying behaviour of droplets from two milk model emulsions with different fat contents was studied in a filament single droplet drying rig. For the higher fat content emulsion, the droplet shrinkage was less distinct and the evaporation process was slower. This was explained by the existence of a hydrophobic fat film, which had occurred at the surface immediately after droplet generation and remained until completion of the drying process. The surface of the low-fat model emulsion droplets also featured an over-stoichiometric amount of fat in respect to the bulk composition, but the absolute surface concentration was lower than the one of protein. The protein further enriched near the surface with increasing drying time, presumably by diffusion due to its surface activity and its lower diffusivity in comparison to lactose, and thus imposed a more hydrophilic, flexible character on the surface shell. This caused the shell of the low-fat model emulsion droplets to be more susceptible to shrinkage and more permeable to allow moisture to evaporate. The study demonstrated the modification of filament single droplet drying by a flash-freezing approach to interrupt the drying process at certain times in order to record the changes in component distribution and chemical surface composition. This enabled correlations between the composition of the developing surface shells and the drying characteristics. The initial surface composition during single droplet drying of the investigated milk model emulsions was found to be consistent with the one of spray-dried milk droplets directly after atomization, which were reported in an earlier study. Therefore, the observed surface formation and its impact on the drying and shrinkage kinetics with proceeding single droplet drying could be considered as representative for a spray drying process under comparable conditions. In future, the proposed methodology can be adopted for other milk emulsions and other food or pharmaceutical particle systems to better understand their respective behaviour during convective drying. Applicability of the obtained results on an industrial spray-drying process will yet depend on whether the surface composition of the generated droplets agrees with the initial state of droplets produced with the corresponding atomization nozzle utilized on industrial scale.

References

[1] B. Adhikari, T. Howes, B.R. Bhandari, T.a.G. Langrish, Effect of addition of proteins on the production of amorphous sucrose powder through spray drying, J. Food Eng. 94 (2009) 144–153, http://dx.doi.org/10.1016/j.jfoodeng.2009.01.029.

[2] S.G. Anema, D.N. Pinder, R.J. Hunter, Y. Hemar, Effects of storage temperature on the solubility of milk protein concentrate (MPC85), Food Hydrocolloids 20 (2006) 386–393.

[3] A.J. Baldwin, G.N.T. Truong, Development of insolubility in dehydration of dairy milk powders, Food Bioprod. Process. 85 (2007) 202–208.

[4] G.S. Bylund, Dairy Processing Handbook, Tetra Pak Processing Systems AB, Lund, 2003.

[5] D.H. Charlesworth, W.R. Marshall, Evaporation from drops containing dissolved solids, AIChE J. 6 (1960) 9–23, http://dx.doi.org/10.1002/aic.690060104.

[6] X.D. Chen, The basics of a reaction engineering approach to modeling air-drying of small droplets or thin-layer materials, Drying Technol. 26 (2008) 627–639, http://dx.doi.org/10.1080/07373930802045908.

[7] X.D. Chen, S.X.Q. Lin, Air drying of milk droplet under constant and time-dependent conditions, AIChE J. 51 (2005) 1790–1799, http://dx.doi.org/10.1002/aic.10449.

[8] X.D. Chen, W. Pirini, M. Ozilgen, The reaction engineering approach to modelling drying of thin layer of pulped Kiwifruit flesh under conditions of small Biot numbers, Chem. Eng. Process. 40 (2001) 311–320, http://dx.doi.org/10.1016/S0255-2701(01)00108-8.

[9] X.D. Chen, G.Z. Xie, Fingerprints of the drying behaviour of particulate or thin layer food materials established using a reaction engineering model, Food Bioprod. Process. 75 (1997) 213–222, http://dx.doi.org/10.1205/096030897531612.

[10] J.H. Chew, N. Fu, T. Gengenbach, X.D. Chen, C. Selomulya, The compositional effects of high solids model emulsions on drying behaviour and particle formation processes, J. Food Eng. (2015), http://dx.doi.org/10.1016/j.jfoodeng.2015.02.007.

[11] J.H. Chew, N. Fu, M.W. Woo, K. Patel, C. Selomulya, X.D. Chen, Capturing the effect of initial concentrations on the drying kinetics of high solids milk using reaction engineering approach, Dairy Sci. Technol. 93 (2013) 415–430, http://dx.doi.org/10.1007/s13594-013-0111-z.

[12] J.H. Chew, W. Liu, N. Fu, T. Gengenbach, X.D. Chen, C. Selomulya, Exploring the drying behaviour and particle formation of high solids milk protein concentrate, J. Food Eng. (2014), http://dx.doi.org/10.1016/j.jfoodeng.2014.07.004.

[13] S.V. Crowley, A.L. Kelly, P. Schuck, R. Jeantet, J.A. O'mahony, Rehydration and solubility characteristics of high-protein dairy powders, in: P.L.H. Mcsweeney, J.A. O'mahony (Eds.), Advanced Dairy Chemistry. Volume 1B: Proteins: Applied Aspects, fourth ed., Springer, Heidelberg, 2016.

[14] A. Einstein, Über die von der molekularkinetischen Theorie der Wärme geforderte Bewegung von in ruhenden Flüssigkeiten suspendierten Teilchen, Ann. Phys. 4 (1905), http://dx.doi.org/10.1002/andp.200590005.

[15] P. Fäldt, B. Bergenståhl, Spray-dried whey protein/soybean oil emulsions. 1. Surface composition and particle structure, Food Hydrocolloids 10 (1996) 421–429, http://dx.doi.org/10.1016/S0268-005X(96)80020-8.

[16] P. Fäldt, B. Bergenståhl, Spray-dried whey protein/lactose/soybean oil emulsions. 2. Redispersability, wettability and particle structure, Food Hydrocolloids 10 (1996) 431–439, http://dx.doi.org/10.1016/S0268-005X(96)80021-X.

[17] P. Fäldt, B. Bergenstahl, G. Carlsson, The surface coverage of fat on food powders analyzed by ESCA (electron spectroscopy for chemical analysis), Food Struct. (USA) 12 (1993) 225–234.

[18] M. Foerster, T. Gengenbach, M.W. Woo, C. Selomulya, The impact of atomization on the surface composition of spray-dried milk droplets, Colloids Surf., B (2016), http://dx.doi.org/10.1016/j.colsurfb.2016.01.012.

[19] N. Fu, Single Droplet Drying of Food and Bacterium Containing Liquids and Particle Engineering, Monash University, 2012.

[20] N. Fu, M.W. Woo, X.D. Chen, Colloidal transport phenomena of milk components during convective droplet drying, Colloids Surf., B 87 (2011) 255–266, http://dx.doi.org/10.1016/j.colsurfb.2011.05.026.

[21] N. Fu, M.W. Woo, S.X. Qi Lin, Z. Zhou, X.D. Chen, Reaction Engineering Approach (REA) to model the drying kinetics of droplets with different initial

sizes – experiments and analyses, Chem. Eng. Sci. 66 (2011) 1738–1747, http://dx.doi.org/10.1016/j.ces.2011.01.009.

[22] C. Gaiani, J. Ehrhardt, J. Scher, J. Hardy, S. Desobry, S. Banon, Surface composition of dairy powders observed by X-ray photoelectron spectroscopy and effects on their rehydration properties, Colloids Surf., B 49 (2006) 71–78, http://dx.doi.org/10.1016/j.colsurfb.2006.02.015.

[23] D.E. Graham, M.C. Phillips, Proteins at liquid interfaces: I. Kinetics of adsorption and surface denaturation, J. Colloid Interface Sci. 70 (1979) 403–414, http://dx.doi.org/10.1016/0021-9797(79)90048-1.

[24] K. Granelli, P. Fäldt, L.Å. Appelqvist, B. Bergenståhl, Influence of surface structure on cholesterol oxidation in model food powders, J. Sci. Food Agric. 71 (1996) 75–82, http://dx.doi.org/10.1002/(SICI)1097-0010(199605)71:1<75::AID-JSFA551>3.0.CO;2-J.

[25] N. Hardas, S. Danviriyakul, J. Foley, W.W. Nawar, P. Chinachoti, Accelerated stability studies of microencapsulated anhydrous milk fat, LWT-Food Sci. Technol. 33 (2000) 506–513, http://dx.doi.org/10.1006/fstl.2000.0696.

[26] F. Helmchen, W. Denk, Deep tissue two-photon microscopy, Nat. Methods 2 (2005) 932–940, http://dx.doi.org/10.1038/NMETH818.

[27] M.K. Keogh, B.T. O'kennedy, J. Kelly, M.A. Auty, P.M. Kelly, A. Fureby, A.M. Haahr, Stability to oxidation of spray-dried fish oil powder microencapsulated using milk ingredients, J. Food Sci. 66 (2001) 217–224. 10.1111/j.1365-2621.2001.tb11320x.

[28] E.H.-J. Kim, X.D. Chen, D. Pearce, Effect of surface composition on the flowability of industrial spray-dried dairy powders, Colloids Surf., B 46 (2005) 182–187, http://dx.doi.org/10.1016/j.colsurfb.2005.11.005.

[29] E.H.-J. Kim, X.D. Chen, D. Pearce, Surface composition of industrial spray-dried milk powders. 2. Effects of spray drying conditions on the surface composition, J. Food Eng. 94 (2009) 169–181, http://dx.doi.org/10.1016/j.jfoodeng.2008.10.020.

[30] E.H.-J. Kim, X. Dong Chen, D. Pearce, On the mechanisms of surface formation and the surface compositions of industrial milk powders, Drying Technol. 21 (2003) 265–278, http://dx.doi.org/10.1081/DRT-120017747.

[31] S.X.Q. Lin, X.D. Chen, Improving the glass-filament method for accurate measurement of drying kinetics of liquid droplets, Chem. Eng. Res. Des. 80 (2002) 401–410, http://dx.doi.org/10.1205/026387602317446443.

[32] S.X.Q. Lin, X.D. Chen, A model for drying of an aqueous lactose droplet using the reaction engineering approach, Drying Technol. 24 (2006) 1329–1334, http://dx.doi.org/10.1080/07373930600951091.

[33] G. Meerdink, Drying of liquid food droplets enzyme inactivation and multicomponent diffusion, Drying Technol. 12 (1994) 981–982, http://dx.doi.org/10.1080/07373939408960007.

[34] M. Mezhericher, A. Levy, I. Borde, Theoretical drying model of single droplets containing insoluble or dissolved solids, Drying Technol. 25 (2007) 1025–1032, http://dx.doi.org/10.1080/07373930701394902.

[35] A. Millqvist-Fureby, U. Elofsson, B. Bergenståhl, Surface composition of spray-dried milk protein-stabilised emulsions in relation to pre-heat treatment of proteins, Colloids Surf., B 21 (2001) 47–58, http://dx.doi.org/10.1016/S0927-7765(01)00183-7.

[36] J.J. Nijdam, T.a.G. Langrish, The effect of surface composition on the functional properties of milk powders, J. Food Eng. 77 (2006) 919–925, http://dx.doi.org/10.1016/j.jfoodeng.2005.08.020.

[37] Y. Nikolova, J. Petit, A. Gianfrancesco, C.F.W. Sanders, J. Scher, C. Gaiani, Impact of spray-drying process parameters on dairy powder surface composition and properties, Drying Technol. (2015), http://dx.doi.org/10.1080/07373937.2015.1060494.

[38] K.C. Patel, X.D. Chen, S. Kar, The temperature uniformity during air drying of a colloidal liquid droplet, Drying Technol. 23 (2005) 2337–2367, http://dx.doi.org/10.1080/07373930500340437.

[39] A. Putranto, X.D. Chen, Z. Xiao, P.A. Webley, Simple, accurate and robust modeling of various systems of drying of foods and biomaterials: a demonstration of the feasibility of the reaction engineering approach (REA), Drying Technol. 29 (2011) 1519–1528, http://dx.doi.org/10.1080/07373937.2011.580407.

[40] M.S. Rahman, Food Properties Handbook, CRC Press, Boca Raton, 2009.

[41] W.E. Ranz, W.R. Marshall, Evaporation from drops Part I, Chem. Eng. Prog. 48 (1952) 141–146.

[42] W.E. Ranz, W.R. Marshall, Evaporation from drops Part II, Chem. Eng. Prog. 48 (1952) 173–180.

[43] C. Sadek, H. Li, P. Schuck, Y. Fallourd, N. Pradeau, C. Le Floch-Fouéré, R. Jeantet, To what extent do whey and casein micelle proteins influence the morphology and properties of the resulting powder?, Drying Technol 32 (2014) 1540–1551, http://dx.doi.org/10.1080/07373937.2014.915554.

[44] C. Sadek, L. Pauchard, P. Schuck, Y. Fallourd, N. Pradeau, C. Le Floch-Fouéré, R. Jeantet, Mechanical properties of milk protein skin layers after drying: understanding the mechanisms of particle formation from whey protein isolate and native phosphocaseinate, Food Hydrocolloids 48 (2015) 8–16, http://dx.doi.org/10.1016/j.foodhyd.2015.01.014.

[45] C. Sadek, P. Schuck, Y. Fallourd, N. Pradeau, C. Le Floch-Fouéré, R. Jeantet, Drying of a single droplet to investigate process-structure-function relationships: a review, Dairy Sci. Technol. (2014) 1–24, http://dx.doi.org/10.1007/s13594-014-0186-1.

[46] P. Schuck, S. Mejean, A. Dolivet, C. Gaiani, S. Banon, J. Scher, R. Jeantet, Water transfer during rehydration of micellar casein powders, Le Lait 87 (2007) 425–432, http://dx.doi.org/10.1051/lait:2007016.

[47] A. Taneja, A. Ye, J.R. Jones, R. Archer, H. Singh, Behaviour of oil droplets during spray drying of milk-protein-stabilised oil-in-water emulsions, Int. Dairy J. 28 (2013) 15–23, http://dx.doi.org/10.1016/j.idairyj.2012.08.004.

[48] D.E. Walton, The evaporation of water droplets. A single droplet drying experiment, Drying Technol. 22 (2004) 431–456, http://dx.doi.org/10.1081/DRT-120029992.

[49] S. Wang, T.a.G. Langrish, A distributed parameter model for particles in the spray drying process, Adv. Powder Technol. 20 (2009) 220–226, http://dx.doi.org/10.1016/j.apt.2009.03.004.

[50] M.W. Woo, W.R.W. Daud, A.S. Mujumdar, M.Z.M. Talib, W.Z. Hua, S.M. Tasirin, Comparative study of droplet drying models for CFD modelling, Chem. Eng. Res. Des. 86 (2008) 1038–1048, http://dx.doi.org/10.1016/j.cherd.2008.04.003.

[51] P. Zhu, K. Patel, S. Lin, S. Méjean, E. Blanchard, X.D. Chen, P. Schuck, R. Jeantet, Simulating industrial spray-drying operations using a reaction engineering approach and a modified desorption method, Drying Technol. 29 (2011) 419–428, http://dx.doi.org/10.1080/07373937.2010.501928.